AIP | The Journal of Chemical Physics

Synthesis of LaF3 nanosheets with high fluorine mobility investigated by NMR relaxometry and diffusometry

L. B. Gulina, M. Schäfer, A. F. Privalov, V. P. Tolstoy, and I. V. Murin

Citation: The Journal of Chemical Physics **143**, 234702 (2015); doi: 10.1063/1.4937415
View online: http://dx.doi.org/10.1063/1.4937415
View Table of Contents: http://scitation.aip.org/content/aip/journal/jcp/143/23?ver=pdfcov
Published by the AIP Publishing

Synthesis of LaF_3 nanosheets with high fluorine mobility investigated by NMR relaxometry and diffusometry

L. B. Gulina,[1] M. Schäfer,[2] A. F. Privalov,[2] V. P. Tolstoy,[1] and I. V. Murin[1]
[1]*Institute of Chemistry of St. Petersburg State University 198504, Universitetsky pr., 26 Peterhof, St. Petersburg, Russia*
[2]*Institut für Festkörperphysik, Technische Universität Darmstadt, Hochschulstr. 6, 64289 Darmstadt, Germany*

(Received 1 October 2015; accepted 25 November 2015; published online 16 December 2015)

Ionically conducting lanthanum fluoride (LaF_3), displaying a nanoscopic lamellar structure, has been synthesized at the surface of an aqueous solution of $LaCl_3$ and HF. The structure and the chemical composition of the conductor have been analyzed by SEM, electron probe microanalysis, X-ray powder diffraction, FTIR, and ^{19}F magic angle spinning nuclear magnetic resonance (NMR) spectroscopy. The fluorine dynamics have been studied by NMR diffusometry and relaxometry in a temperature range from room temperature up to 875 K. The fluorine self-diffusion coefficient of the nanostructured LaF_3 is about two orders of magnitude larger than that of bulk LaF_3. This novel material is highly promising for many typical applications of fluorine ionic systems. © *2015 AIP Publishing LLC*. [http://dx.doi.org/10.1063/1.4937415]

I. INTRODUCTION

Compared to a homogeneous bulk sample, nanostructured materials often possess striking new characteristics, enabling advanced applications and enhanced material properties.[1] Lanthanum fluoride LaF_3 is a crystalline material displaying ionic conductivity in its fluorine lattice, which has numerous domains of application, e.g., in sensors,[2–4] luminescence,[5,6] and superionic conductors.[7–10]

Several methods to synthesize LaF_3 with a nanoscopic structured morphology are known: hydrothermal,[11] microwave[12] and high temperature syntheses,[13] as well as the liquid-solid-solution technique.[14] Surface active substances are employed to control the particle size.[15] To synthesize LaF_3 in the form of nanolayers, successive ionic layer deposition,[16] vacuum sublimation[17] or metalorganic chemical vapor deposition[18] have been used. In common, all these methods are complicated and expensive.

A promising alternative developed by our group is the synthesis at an air-solution interface.[19] The interaction of gaseous hydrogen fluoride HF with the surface of an aqueous solution of the lanthanum salt $LaCl_3$ and the hydrochloric acid HCl can be exploited to produce a LaF_3 layer with a thickness of the order of 1 μm featuring an ordered lamellar substructure on the nanometer scale (nanosheets). During the process of drying the material, this layer is found to break into smaller pieces which roll into microtubules. A similar technique was applied to prepare microtubules of various inorganic compounds: for example $H_xMnO_2{\cdot}nH_2O$[20,21] and $As_2S_3{\cdot}nH_2O$.[22] The advantages of this synthesis method are as follows: it takes place in soft chemistry conditions at moderate temperature; the equipment is comparatively simple; no surfactants or solid state matrices are required.

The study of ionic mobility in the nanostructured sheets of LaF_3 and its comparison with that of the bulk is of great interest. NMR is an appropriate method for such a study.

NMR is sensitive to structural properties as well as to dynamics on the microscopic level (line shape and the spin-lattice relaxation)[23,24] but can also be used to measure dynamics on a macroscopic scale (diffusometry).[25]

Ion dynamics in bulk LaF_3 were explored in Refs. 26–29. In small clusters with dimensions of a few nanometers, surface effects can be of great importance in ionic systems.[30] In particular, higher fluorine mobility may be expected in the nanostructured samples compared to that of bulk LaF_3.[31,32] The nanosize effects of layered fluorine superionic conductors were investigated by molecular dynamics simulations.[33] Comparison of dynamic properties in nanostructured materials with those in their bulk counterparts is an established way to study the peculiarities of nanosized materials.[34–38] This will also be done in the present work.

The objective of this work is twofold: The characterization of the structure and chemical composition and the investigation of the fluorine ion dynamics in LaF_3 nanosheets synthesized at the air-solution interface and to compare it with that of bulk LaF_3.

The characterization was done using several methods: scanning electron microscopy (SEM), electron probe microanalysis (EPMA), Fourier transform infrared spectroscopy (FTIR), X-ray powder diffraction (XRPD), and ^{19}F magic angle spinning (MAS) nuclear magnetic resonance (NMR) spectroscopy.

Fluorine dynamics was investigated by NMR diffusometry in a static field gradient (SFG) and by spin-lattice relaxometry (SLR).

II. EXPERIMENTAL

A. Synthesis

The synthesis was performed under steady-state conditions at room temperature in a hermetically closed 50 ml Teflon

reactor. Two open vessels with an aqueous 0.05M solution of $LaCl_3$ and 40% HF were placed nearby. The surface area of the solutions was 8 cm^2 and 4 cm^2, respectively. Deionized water with an electrical resistivity higher than 18 MΩ cm was used for the preparation of the solutions. Concentrated HCl was used to acidify the $LaCl_3$ salt solution.

After treating the aqueous solution with gaseous HF for at least 30 min, a thin film was obtained on the surface of the salt solution. This layer was transferred to a clean water surface using a special "spoon" to remove the remainings of the solution.

After 10 min, the water was renewed. This procedure was repeated 3 times. Subsequently, the layer was transferred to a monocrystalline silicon substrate and dried at room temperature. The substrates were prepared in the following way: First, they were cleaned with acetone, then kept for 10 min in an ultrasonic cleaner (60 W) filled with "piranha solution," consisting of hydrogen peroxide H_2O_2 and concentrated sulfuric acid H_2SO_4 of a volume ratio of 3:7. Finally, they were carefully washed with water. More details on the synthesis procedure can be found in Ref. 39.

B. Structure

SEM was performed using a Zeiss Merlin scanning electron microscope. Images were recorded applying an acceleration voltage of 2 kV. Immediately after the synthesis, the layer was dried and investigated from all sides. Furthermore, the morphology was examined after the layer was heated to high temperatures with a heating rate of 5 K/min and kept in a furnace for 10 min.

By EPMA, we analyzed the chemical composition of the layer surface. The measurements were performed using an Oxford Instruments INCA x-act detector. The acceleration voltage was 10 kV.

FTIR spectroscopy was carried out on a Bruker Vertex 70 spectrometer. In preparing the measurement, the sample was triturated in acetone and a monocrystalline silicon surface was coated with the resulting suspension. Then the spectrum was recorded in a differential mode with a silicon surface as a reference. 64 scans were accumulated. The resolution was 4 cm^{-1}.

After the sample was ground to a homogeneous powder, mixed with vaseline, and located on a SiO_2 support, XRPD was applied on a Rigaku MiniFlex II diffractometer using the Cu K_α-line as a source of monochromatic X-ray radiation. The beam angles were varied in the range from 2° to 120°.

Highly resolved solid state ^{19}F NMR spectra were obtained using a BRUKER 70 kHz MAS probe with a 1.3 mm rotor at a ^{19}F Larmor frequency of ν_L = 565 MHz (^1H Larmor frequency ν_L = 600 MHz). We used sample spinning up to 50 kHz. To distinguish and to eliminate the rotational sidebands, the spectra were recorded additionally at 30 and 40 kHz. All spectra were recorded at room temperature. They resulted from the Fourier transformation of free induction decays after a 90° pulse of 2 μs. ^{19}F chemical shifts were referenced to neat $CFCl_3$ (δ = 0.0 ppm).

After the synthesis, the samples can preserve some residual water. Because the signal amplitude is proportional to the number of excited nuclei, NMR is able to estimate the quantity of protons relative to the fluorine nuclei by measuring the ^1H and ^{19}F intensities under the same conditions. NMR analysis of the water content was carried out using a NMR magnet with a very high static magnetic field gradient (SFG).[40] This magnet is specifically designed to produce a large field inhomogeneity, which is realized by an antiparallel arrangement of superconducting field coils. One can detect the ^{19}F and the ^1H signals at the same frequency individually only by changing the position of the probe in the gradient. The ratio of these signal amplitudes contains the information about the water content in the sample.

C. Dynamics

The temperature dependence of the self-diffusion coefficient of the fluorine ions was quantified by SFG NMR diffusometry[40] in a wide temperature range up to 875 K. A three pulse stimulated echo sequence was applied. In the case of normal Gaussian diffusion, the resulting NMR echo amplitude S can be described by[40]

$$S \approx \exp\left(-\left(\frac{t_m}{T_1}\right)^{\beta}\right)\exp\left(-\frac{2\tau}{T_2}\right)\exp\left(-D\gamma^2 g^2 \tau^2\left(\frac{2}{3}\tau + t_m\right)\right), \quad (1)$$

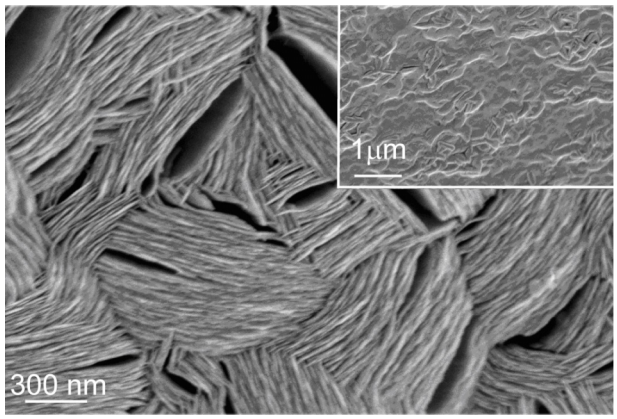

FIG. 1. SEM image of a LaF_3 layer in front view from the solution side (main image) and the air side (inset).

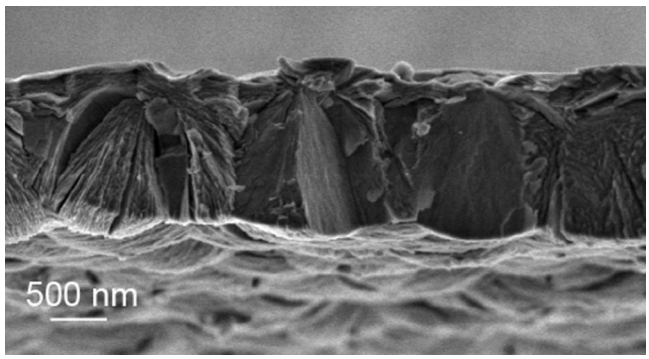

FIG. 2. SEM image of a LaF_3 layer in side view.

where D is the diffusion coefficient, t_m is the mixing time which describes the storage duration of the magnetization in the z-direction after the second RF pulse, τ is the evolution time for dephasing after the first RF pulse and for rephasing after the third pulse, T_1 and T_2 are the spin-lattice and the spin-spin relaxation times, respectively, γ is the gyromagnetic ratio, g is the field gradient, and β is the relaxation stretching parameter.

By using a 2 kW power amplifier, short 90°-pulse lengths of 0.4 μs have been achieved, leading to a broad frequency band for the spin excitation. The experiments were performed at ν_L = 140 MHz and the gradient of the magnetic field was g = 120 T/m.

The ^{19}F spin lattice relaxation time T_1 at ν_L = 140 MHz was measured applying a saturation recovery pulse sequence. A temperature range up to 875 K was covered using a specially designed high-temperature probe.[41] While at high temperatures, the absolute temperature could be specified within ±10 K, the long term temperature stability was of the order of 1 K.

III. RESULTS AND DISCUSSION

A. Morphology, size, and structure

SEM has shown (Fig. 1) that the LaF_3 layers consist of ordered arrays of nanosheets, most of which are oriented perpendicular to the layer surface. From the bottom (solution) side, the density of the nanosheets appears lower than from the top (air) side, as one can see in the inset of Fig. 1 and in Fig. 2.

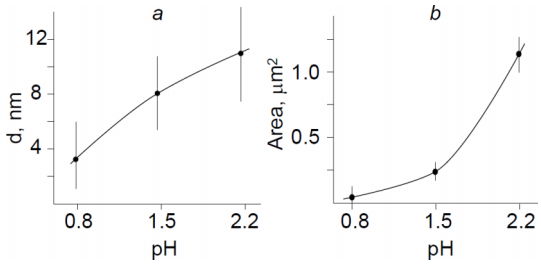

FIG. 3. Dependence of the thickness (a) and surface area (b) of the LaF_3 nanosheets on the pH-value of the lanthanum salt solution.

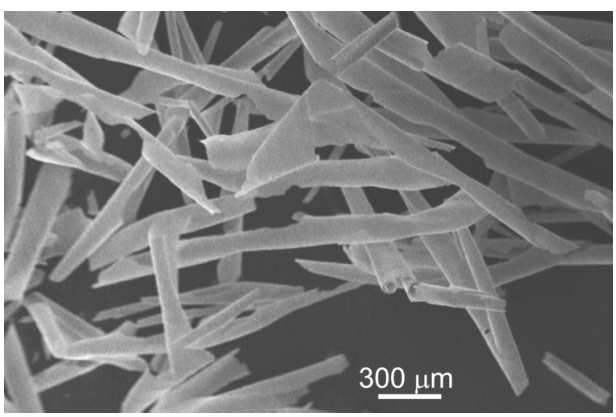

FIG. 4. SEM image of LaF_3 microtubules formed after drying.

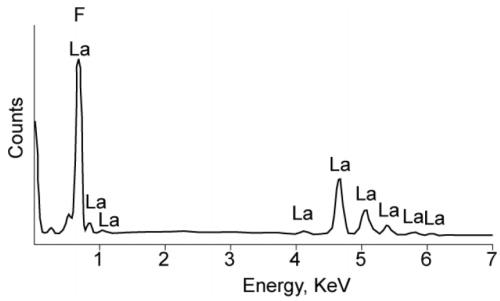

FIG. 5. EPMA spectrum of the LaF_3 layer.

The average thickness of the layer can be estimated as 1.5 μm. The thickness of the nanosheets is about 10-12 nm and their surface area varies from 1.0 μm^2 to 1.5 μm^2 (Fig. 2).

The pH-value of the solution was varied to study its influence on the size of the nanosheets. An increase of the pH-value from 0.8 to 2.2 leads to an increase of the thickness from 3 nm to 11 nm (Fig. 3). The surface area of the sheets increases by one order of magnitude.

The calculations were performed using "Digital Micrograph program" (Gatan, Inc.).

The formation of the nanosheets can be described in the following way: After the reaction of HF gas and $LaCl_3$ solution, LaF_3 nanocrystals form on the surface of the liquid. These crystals block the penetration of HF into the solution of lanthanum salt. In the inset of Fig. 1, one can see the dense packing of these crystals from the gas side. The penetration of HF is still only possible between the crystals, where further growth perpendicular to the solution surface occurs, forming the nanosheets.

After drying, the layer breaks into fragments which roll into microtubules (Fig. 4). The dimensions of these tubules are affected by the synthesis and can vary from 20 μm to 100 μm in thickness and from 400 μm to 2 mm in length.

The sample shown in Figs. 1, 2, and 4 was investigated by NMR.

EPMA confirmed that no chlorine atoms from the aqueous solution of $LaCl_3$ and HCl are present. The element composition of the layer consists only of La and F atoms. The results are presented in Fig. 5.

FTIR spectroscopy has shown an absorption line at 352 cm^{-1}. This line can be attributed to valence fluctuations of La-F bonds in LaF_3.[42] In addition to this, absorption lines with maxima at 3400 cm^{-1} and 1630 cm^{-1} are found, which are related to water O–H bonds (Fig. 6). This indicates that water

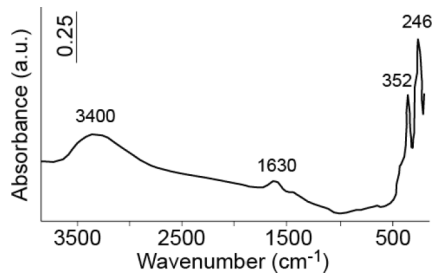

FIG. 6. FTIR spectrum of the LaF_3 layer.

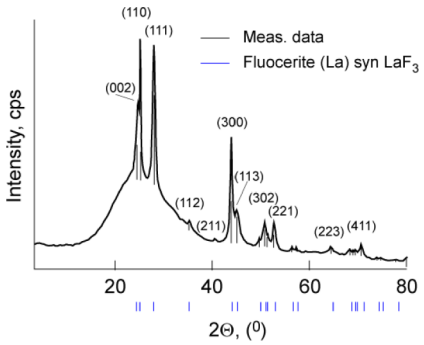

FIG. 7. XRPD pattern of the LaF_3 layer. A broad halo in the 2θ range of 23° is due to the SiO_2 substrate.

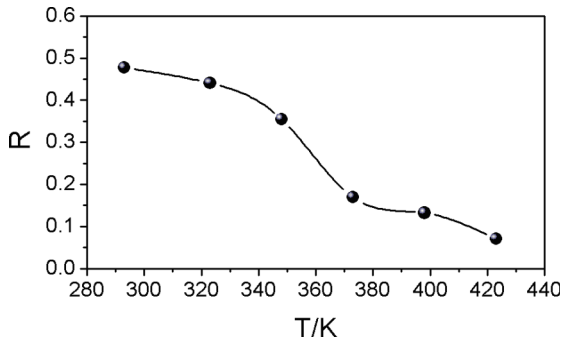

FIG. 9. The ratio R of signal intensities $^1H/^{19}F$ as a function of temperature.

is present in the sample after the synthesis and preliminary drying. For bulk LaF_3, it is known that solvation on the surface forms a 20 nm thick layer containing water molecules.[43]

XRPD analysis (Fig. 7) has indicated that the nanosheets consist of LaF_3 revealing a trigonal tysonite crystal structure with the spatial group $P\bar{3}c1$.[44] No further peaks related to other compounds were detected. In the pattern it is possible to detect broad features of low intensity of the 001 reflection profiles, such as 002, 112, 113, and 223. As known, a peak broadening can be related to the crystallite size and a lattice strain due to dislocations. Sharp reflections are observed in the h00 and hk0 planes (sheet surfaces). Thus, the XRD pattern can be interpreted as the sum of detectable peaks with various widths which characterize the anisotropy of 2D nanocrystals. This result is in agreement with SEM imaging of the sample (Figs. 1 and 2).

Due to the synthesis method, our samples inevitably contain water, as has been shown by FTIR spectroscopy.

The water content and its loss with increasing temperature were estimated from the ratio R between the ^1H and the ^{19}F NMR echo amplitudes obtained from measurements at the same frequency for both nuclei. This is achieved by a proper repositioning of the sample signal intensities measured in a magnetic field gradient of 80 T/m (Fig. 8). Gyromagnetic ratios for protons and fluorine were taken into account.

In the initial state after preliminary drying, the ratio $^1H/^{19}F$ was around 0.5, which corresponds to the initial composition $(LaF_3)_{0.6}(H_2O)_{0.4}$. During the heating, a gradual reduction of the water content was observed (Fig. 9). The sample was kept at each temperature for one day. After heating to 425 K, the $^1H/^{19}F$ ratio dropped below 0.1. Heating to higher temperatures leads to an almost complete disappearance of the ^1H signal.

To verify whether the crystal structure of the nanosheets is similar to that of a bulk material, we compared the corresponding MAS spectra (Fig. 10). The bulk spectrum consists of three lines, which can be assigned to the three known structurally non-equivalent fluorine sublattices of tysonite, denoted as F_1, F_2, and F_3. Their isotropic chemical shifts are in good agreement with Ref. 45, where they are specified as $\delta(F_1) = -23.6$ ppm, $\delta(F_2) = 25.3$ ppm, and $\delta(F_3) = 16.9$ ppm. The spectrum of the nanostructured sample significantly differs from that of the bulk sample (Fig. 10).

All lines have a full width at half maximum (FWHM) of about 10 kHz. It is much broader than that of the bulk, where the FWHM is of about 2.5 kHz. The F_1 line is found at the expected position. The F_2 and the F_3 lines cannot be resolved. In the spectrum of nanostructured LaF_3, another broad contribution with about 4% of intensity at about 3 ppm can be seen. The origin of this line is not evident, but it vanishes at higher temperatures. Probable candidates can be a layer of LaF_2OH or $LaF(OH)_2$ on the surface of LaF_3 in the presence of water.[43] Also associates of $(HF)_n(H_2O)_m$ on the surface can be considered.[46]

The broadened MAS NMR lines in the nanostructured sample are not surprising. One can assume that surface effects

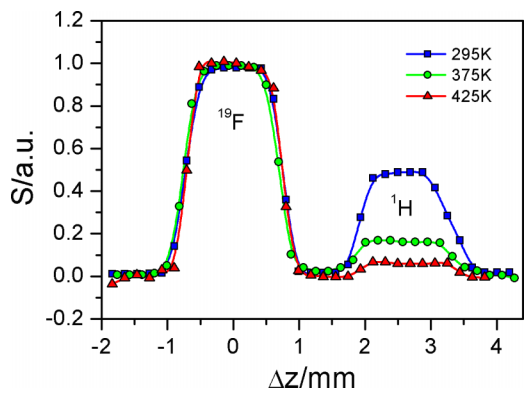

FIG. 8. Normalized NMR signal intensity dependent on the sample position in the gradient magnet at 80 T/m (rectangular sample tube).

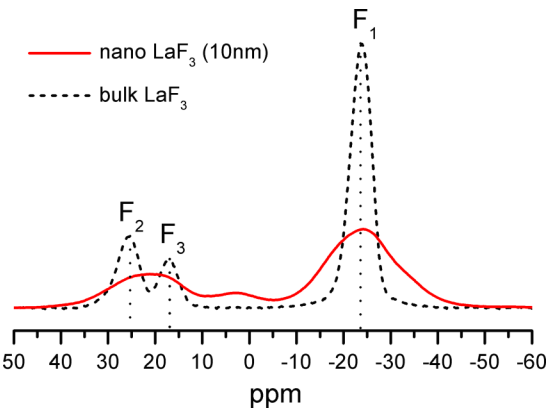

FIG. 10. MAS NMR spectra of bulk and 10 nm thin nanosheets of LaF_3. Dotted lines show the isotropic chemical shifts taken from Ref. 45. The reference is $CFCl_3$, 8 scans, repetition time 10 s, MAS frequency 50 kHz.

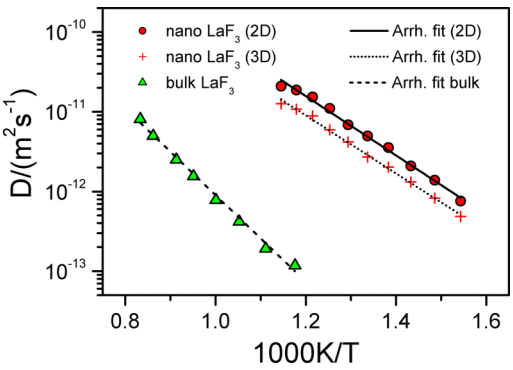

FIG. 11. Arrhenius plot of diffusion coefficients of the nanostructured (10 nm) LaF_3, determined under the assumption of a 2D and 3D models, and diffusion coefficients of the bulk LaF_3.

are involved, such that a high fraction of fluorine ions are located at the surface having different local environments. This necessarily leads to the observed distribution of the isotropic chemical shift. Similar phenomena are known from NMR on nano-particles, which often display broadened resonances due to positional variation of the local electronic and structural environment.[47–49]

B. Dynamics

Our NMR results using SFG NMR indicate that the ^{19}F ion mobility in the nanostructured LaF_3 is significantly higher than that of the bulk. Self-diffusion coefficients of the 10 nm thin nanosheets are about two orders of magnitude larger, see Fig. 11. The diffusion coefficients of the bulk LaF_3[26] are presented for comparison. The temperature dependence of the diffusion coefficients can be well described by an Arrhenius law for both samples. The activation energy for the nanostructured sample is (0.72 ± 0.03) eV, while for the bulk sample, it is (1.10 ± 0.05) eV.

To eliminate the impact of relaxation on the echo damping and to prove that the diffusion coefficients are independent of the diffusion time at each temperature, we performed stimulated echo measurements at various mixing times t_m (Fig. 12). All data are globally fitted using Eqs. (1) and (2). We performed a similar experiment varying t_m for different evolution times τ (Fig. 13). The diffusion coefficients

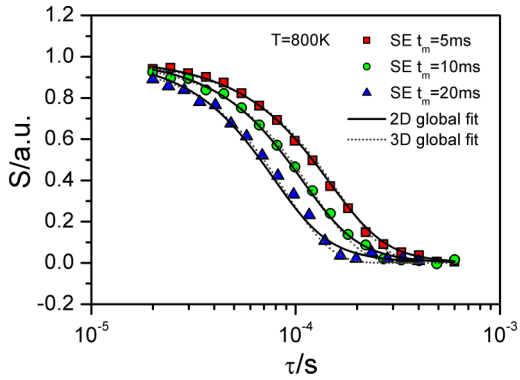

FIG. 12. Dependence of the magnetization decay on the evolution time τ for the stimulated echo with different mixing times t_m. The solid lines stem from a global fit.

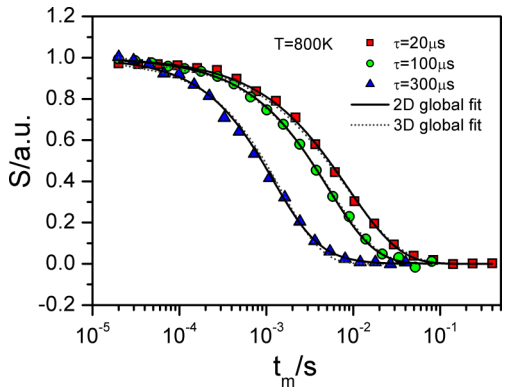

FIG. 13. Dependence of the magnetization decay on the mixing time t_m for the stimulated echo with different evolution times τ. The solid lines stem from a global fit.

presented in Fig. 11 result from a global fit of all data sets.

For the following two reasons, we see in our experiments 2D diffusion: First, typical diffusion times, which are in the ms range, are much longer than those which a single ion needs to diffuse perpendicular to the surface of a sheet. Therefore, even at short diffusion times we are sensitive to ionic motion along the sheets only. Second, our diffusion times are not long enough to trace the ionic motion over distances longer than typical sheet lengths of about 1 μm. (Of course, as seen from Fig. 2, there is a broad size distribution such that some ions will either experience restricted diffusion or leave their sheet.) Therefore, not only at short but also at long diffusion times we are sensitive to motion along the sheets only. Thus, we see an effective unrestricted 2D diffusion. Despite these arguments which strongly call for the 2D scenario, we include in Fig. 11, only for comparison, the diffusion coefficients determined under the assumption of a 3D model. As seen from the figure, there is less than a factor of 2 between the two models.

For 2D diffusion, the resulting diffusion dependent term of the signal amplitude S can be described by Eq. (2) for the case $t_m >> \tau$,[25]

$$S_{2D} \approx \int_0^1 \exp(q^2 D t_m (x^2 - 1))dx, \qquad (2)$$

where $q = \gamma g \tau$ is the generalized scattering vector.[40]

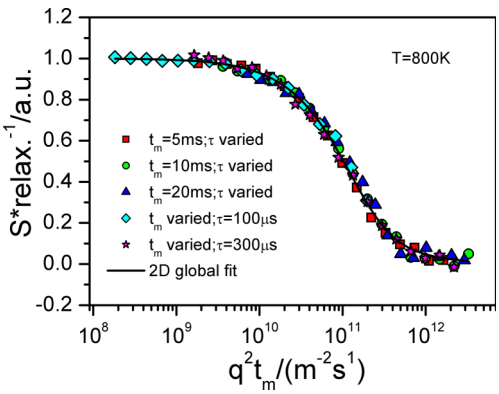

FIG. 14. Master curve of the stimulated echos with various evolution and mixing times at 800 K.

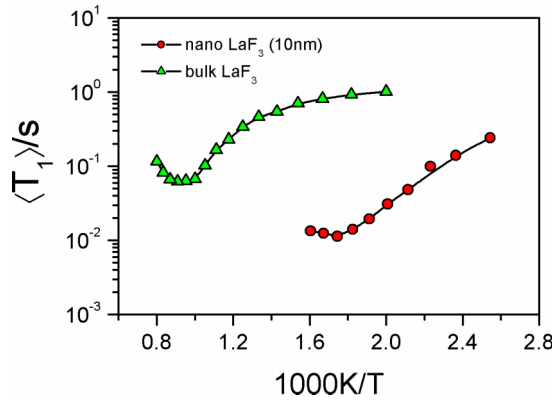

FIG. 15. Temperature dependence of T_1 for the nanostructured (10 nm) and bulk LaF_3.

All magnetization curves can be well described by a single master curve (Fig. 14) plotted over $q^2 t_m$. The good agreement of the results measured at various times confirms the assumption of normal diffusion without further restriction effects.

The faster dynamics in the nanostructured LaF_3 is confirmed by the spin lattice relaxation measurements. A minimum in T_1 (indicating the correlation time of ionic jumps $\tau_c \approx 7 \times 10^{-10}$ s) occurs at comparatively low temperature of about 600 K, while for the bulk sample at about 1100 K (Fig. 15).

We should mention that the magnetization curves in nanosized material can be described by the stretched exponential Kohlrausch-Williams-Watts (KWW) function. In Fig. 11, mean spin lattice relaxation times are presented. The stretching parameter β in the KWW function is about 0.6, while the relaxation in bulk LaF_3 is mono-exponential in all temperature ranges in agreement with Ref. 26. Usually, such a low β reflects strong motional heterogeneity, which is not surprising for structurally disordered nanosized LaF_3.

IV. CONCLUSION

We can conclude that there are prospects for a new class of 2D nanocomposite materials on the basis of LaF_3 with enhanced ionic conductivity.

The synthesis on the air-solution interface requires low operational costs and constitutes a convenient method for the synthesis of nanosized fast superionic conductor LaF_3.

The synthesized material consists of LaF_3 in composition with water $(LaF_3)_{0.6}(H_2O)_{0.4}$. At temperatures above 425 K, residual water disappears. The resulting LaF_3 features a lamellar structure composed of about 10 nm thin nanosheets. It shows enhanced fluorine dynamics with diffusion coefficients of about two orders of magnitude higher than that of the bulk and a T_1 minimum at significantly lower temperature.

Our experiments have demonstrated the possibility of studying fluorine ionic diffusion on the interface of nanostructured materials by NMR.

The structural as well as dynamical disorders are registered by ^{19}F MAS NMR and by the stretched spin lattice relaxation behaviour.

In the near future, we will further investigate dynamic properties from the nanostructured LaF_3 with varying layer thickness.

Nanostructured materials provide the perspective for many applications typical for fluorine ionic systems: chemical sensors, condensers, and ion batteries not only as bulk but also as thin-film systems.

ACKNOWLEDGMENTS

The study was supported by a grant of St. Petersburg State University, research Project No. 12.38.259.2014. The XRD research was carried out by the X-ray Diffraction Centre of St. Petersburg State University. The SEM study was carried out by the Nanotechnology Centre of St. Petersburg State University. The NMR experiments were accomplished in the Institute of Solid State Physics and the Institute of Physical Chemistry, Technical University Darmstadt.

[1]J. Schoonman, Solid State Ionics **135**, 5 (2000).
[2]S. Harke, H.-D. Wiemhöfer, and W. Göpel, Sens. Actuators **B1**, 188 (1990).
[3]L. Bartholomaus and W. Moritz, Solid State Ionics **132**, 31 (2000).
[4]S. Guha and S. Saha, J. Am. Chem. Soc. **132**, 17674 (2010).
[5]H. Hu, Z. Chen, T. Cao, Q. Zhang, M. Yu, F. Li, T. Yi, and C. Huang, Nanotechnology **19**, 375702 (2008).
[6]C. Li, X. Liu, P. Yang, C. Zhang, H. Lian, and J. Lin, J. Phys. Chem. C **112**, 2904 (2008).
[7]I. Brach and H. Schulz, Solid State Ionics **15**, 135 (1985).
[8]I. V. Murin, F. Fujara, O. V. Glumov, A. F. Privalov, and H.-M. Vieth, Mater. Sci. Forum **239-241**, 407 (1997).
[9]J. Schoonman, G. Oversluizen, and K. E. D. Wapenaar, Solid State Ionics **1**, 211 (1980).
[10]A. Kessler, R. Hoger, and I. V. Murin, Mater. Res. Bull. **16**, 1185 (1981).
[11]X. Yang, X. Dong, J. Wang, and G. Liu, J. Alloys Compd. **487**, 298 (2009).
[12]D. S. Jacob, L. Bitton, J. Grinblat, I. Felner, Yu. Koltypin, and A. Gedanken, Chem. Mater. **18**, 3162 (2006).
[13]Y. Tian, X. Jiao, J. Zhang, N. Sui, D. Chen, and G. Hong, J. Nanopart. Res. **12**, 161 (2010).
[14]X. Wang, J. Zhuang, Q. Peng, and Y. Li, Nature **437**, 121 (2005).
[15]G. Wang, Q. Peng, and Y. Li, Acc. Chem. Res. **44**, 322 (2011).
[16]B. S. Zhuchkov, V. P. Tolstoy, and I. V. Murin, Solid State Ionics **101-103**, 165 (1997).
[17]F. Labidi, J. Morcos, and J. Salardenne, Solid State Ionics **34**, 1 (1989).
[18]G. G. Condorelli, S. Gennaro, and I. L. Fragala, Chem. Vap. Deposition **6**, 185 (2000).
[19]L. B. Gulina and V. P. Tolstoy, Russ. J. Gen. Chem. **84**, 1472 (2014).
[20]V. P. Tolstoi and L. B. Gulina, Russ. J. Gen. Chem. **83**, 1635 (2013).
[21]V. P. Tolstoy and L. B. Gulina, Langmuir **30**, 8366 (2014).
[22]V. P. Tolstoy and L. B. Gulina, J. Nano- Electron. Phys. **5**, 01003 (2013).
[23]N. Bloembergen, E. M. Purcell, and R. V. Pound, Phys. Rev. **73**, 679 (1948).
[24]M. H. Levitt, *Spin Dynamics: Basics of Nuclear Magnetic Resonance* (John Wiley & Sons, Chichester, 2001).
[25]P. T. Callaghan, *Principles of Nuclear Magnetic Resonance Microscopy* (Oxford University Press, Oxford, 1991).
[26]M. A. Denecke, W. Gunsser, A. F. Privalov, and I. V. Murin, Solid State Ionics **52**, 327 (1992).
[27]A. F. Privalov, H.-M. Vieth, and I. V. Murin, J. Phys. Chem. Solids **50**, 395 (1989).
[28]A. F. Aalders, A. F. M. Arts, and H. W. De Wijn, Phys. Rev. B **32**, 5412 (1985).
[29]F. Fujara, D. Kruk, O. Lips, A. F. Privalov, V. Sinitsyn, and H. Stork, Solid State Ionics **179**, 2350 (2008).
[30]J. Maier, Chem. Matter. **26**, 348 (2014).
[31]P. Heitjans and M. Wilkening, Defect Diffus. Forum **283-286**, 705 (2008).
[32]V. I. Bulatov, R. W. Grimes, and A. H. Harker, JOM-e **49**, 4 (1997).
[33]K. Nomura and M. Kobayashi, Ionics **14**, 131 (2008).
[34]P. Heitjans and M. Wilkening, MRS Bull. **34**, 915 (2009).
[35]A. V. Chadwick and S. L. P. Savin, Solid State Ionics **177**, 3001 (2006).
[36]J. Schoonman, Solid State Ionics **157**, 319 (2003).

[37]X. Guo and J. Maier, Adv. Mater. **21**, 2619 (2009).
[38]J. Maier, J. Electroceram. **34**, 69 (2015).
[39]L. B. Gulina, V. P. Tolstoy, I. A. Kasatkin, and Y. V. Petrov, J. Fluorine Chem. **180**, 117 (2015).
[40]I. Chang, F. Fujara, B. Geil, G. Hinze, H. Sillescu, and A. Tolle, J. Non-Cryst. Solids **674**, 172 (1994).
[41]A. F. Privalov and O. Lips, Appl. Magn. Reson. **22**, 597 (2002).
[42]V. P. Tolstoy, I. V. Chernyshova, and V. A. Scryshevsky, *Handbook of Infrared Spectroscopy of Ultrathin Films* (Wiley-Interscience, New Jersey, 2003), p. 676.
[43]R. De Marco, P. C. Hauser, R. W. Cattrall, J. Liesegang, and G. L. Nyberg, Surf. Interface Anal. **14**, 463 (1989).
[44]The International Centre for Diffraction Data, JCPDS Card No. 00-032-0483.
[45]A. Sadoc, M. Body, C. Legein, M. Biswal, F. Fayon, X. Rocquefelte, and F. Boucher, Phys. Chem. Chem. Phys. **13**, 18539 (2011).
[46]B. Baburao, D. P. Visco, Jr., and T. V. Albu, J. Phys. Chem. A **111**, 7940 (2007).
[47]A. M. Thayer, M. L. Steigerwald, T. M. Duncan, and D. C. Douglass, Phys. Rev. Lett. **60**(25), 2673 (1988).
[48]M. Tomaselli, J. L. Yarger, M. Bruchez, R. H. Havlin, D. deGraw, A. Pines, and A. P. Alivisatos, J. Chem. Phys. **110**(18), 8861 (1999).
[49]S. Cadars, B. J. Smith, J. D. Epping, S. Acharya, N. Belman, Y. Golan, and B. F. Chmelka, Phys. Rev. Lett. **103**(13), 136802 (2009).